Electron channelling contrast imaging of dislocations in a conventional SEM

Pang, Bo; Jones, Ian; Millett, Jeremy C F; Whiteman, Glenn; Chiu, Yu-Lung

DOI:
10.1080/14786435.2016.1262971

Document Version
Peer reviewed version

Citation for published version (Harvard):
Pang, B, Jones, I, Millett, JCF, Whiteman, G & Chiu, Y-L 2016, 'Electron channelling contrast imaging of dislocations in a conventional SEM', *Philosophical Magazine*, vol. 97, no. 5, pp. 346-359. https://doi.org/10.1080/14786435.2016.1262971

Electron channelling contrast imaging of dislocations in a conventional SEM

Journal:	*Philosophical Magazine & Philosophical Magazine Letters*
Manuscript ID	TPHM-16-Jun-0278.R1
Journal Selection:	Philosophical Magazine
Date Submitted by the Author:	13-Oct-2016
Complete List of Authors:	Pang, Bo; University of Birmingham, School of Metallurgy and Materials Jones, Ian P; University of Birmingham, School of Metallurgy and Materials Chiu, Yu lung; University of Birmingham, School of Metallurgy and Materials Millett, Jeremy; AWE Whiteman, Glenn; AWE
Keywords:	electron channelling, electron microscopy, dislocations, tantalum, computer simulation, crystal defects, defect analysis
Keywords (user supplied):	

Electron channelling contrast imaging of dislocations in a conventional SEM

Bo Pang[1], Ian Jones[1], Yu-Lung Chiu[1], Jeremy Millett[2], Glenn Whiteman[2]

School of Metallurgy and Materials, University of Birmingham, Birmingham, United Kingdom[1]

AWE, Aldermaston, Reading, United Kingdom[2]

E-mail: b.pang1989@gmail.com

Electron channelling contrast imaging of dislocations in a conventional SEM

Dislocations in shock loaded tantalum single crystals were imaged using both TEM and ECCI in an SEM with a conventional backscattered electron detector. The results were compared with backscattered electron intensity profiles across dislocations calculated via the dynamic theory of electron diffraction. A one-to-one correspondence between ECCI and TEM is established. High voltage and low index reflections should be used to obtain the highest dislocation contrast and greatest imaging depth.

Keywords: electron channelling; electron microscopy; dislocations; tantalum; computer simulation; crystal defects; defect analysis

Introduction

Electron channelling results from the interaction of high energy electrons with crystalline materials [1]. It can be used to examine the crystallography of a crystal in the scanning electron microscope (SEM) and to characterise the defects within the crystals. The possibility of observing crystal defects using ~~ECCI~~an electron channelling contrast image (ECCI) was predicted in 1962 by Hirsch et al. [2]. An early observation of electron channelling contrast in an SEM was reported by Coates in 1967 [3]. The rapid change of backscattered electron intensity near the Bragg condition was explained in 1970 [4] by Hirsch and Humphreys as an electron channelling effect. In 1972, Spencer et al. [5] developed a full description of the dynamic theory of the channelling contrast of a crystal containing defects, predicting the visibility and invisibility of dislocations in the backscattered electron image. In 1979, Morin et al. made the first observation of dislocations by ECCI, using an SEM with a field emission gun [6]. Experimental results on silicon by Czernuszka et al. in 1990 suggested that the $g \cdot b = 0$ invisibility criterion can be applied to screw dislocations [7]. Image simulations carried out by Wilkinson et al. [8] and Wilkinson and Hirsch [9] indicate that the usual $g \cdot b = 0$ invisibility criterion holds for ECCI. ~~Acceptable dislocation contrast from ECCI~~This invisibility

was ~~found in some cases to be generated within~~ $1\mu m$ ~~from the specimen surface [8].~~ ~~Later~~confirmed by experimental work by Crimp [10~~,~~]. . Experimental work [11] shows that the ECCI can reveal dislocations at a small depth in the specimen (normally a few extinction distances).

ECCI contrast is sensitive to the deviation parameter s. It was reported that the image contrast is optimised at the condition $s \approx 0$ [12] and changes rapidly, particularly when s becomes negative [13]. Simulations by Wilkinson and Hirsch [9] showed that the stress relaxation of a dislocation close to the crystal surface has a minor effect only on the electron channelling contrast image. Therefore, in the numerical calculation of dislocation contrast profiles, it is reasonable to use the crystal displacement of a dislocation in an infinite medium.

There have been many attempts to confirm the contrast of crystal defects in the ECCI using a transmission electron microscope (TEM). Zauter [14] [15] used ECCI to image the sub-grain structure of austenitic stainless steel after fatigue. The sub-grains in the ECCI taken from bulk specimens show many similarities with the TEM micrographs. Weidner [16] [17] compared ECCI of individual dislocation lines from the electron opaque area of a TEM specimen with the TEM image from an electron transparent area of the same specimen. Similar features such as micro twins, long dislocation lines and tangles were observed. Zaefferer [18] made a direct comparison of ECCI and TEM images from the same area of a TWIP steel TEM sample. The stacking faults from ECCI match perfectly well with TEM, although there are a few steeply inclined dislocations only shown in their images. In this paper, ECCI and TEM micrographs from a high dislocation density area have been compared in order to reveal the effect of image depth on the visibility in ECCI of dislocation lines.

ECCI has been used as an efficient tool for measuring dislocation density. Crimp [~~14~~19] carried out an in-situ experiment on a titanium alloy. In his study, dislocation densities were measured by counting the dislocation terminations in the image. A different method was employed by Gutierrez-Urrutia and Raabe [~~15~~20] who counted the number

of dislocation lines N intersecting a grid with a total length L in the ECC image. The contrast depth t calculated by Wilkinson et al. [8] was used as the thickness of the specimen and dislocation density was calculated using the relationship $\rho = 2N/Lt$ [~~15].~~20]. The depth t is the imaging depth of ECCI. Wilkinson [9] performed an image simulation on silicon with an electron beam voltage 40 keV and a reflection vector 220. The limiting depth of the imaging was around $5\xi_g$ (~250 nm). Zaefferer obtained similar results on the simulation of stacking fau~~lts~~ images [18], but, experimentally, Zaefferer found that this depth varies between 50 and 100 nm, based on the SEM conditions. This limits any comparison of maximum imaging depth for different materials, reflections, or even different experimental conditions (e.g. different detector, beam current, etc). The influence of these experimental conditions on the usable image depth is discussed in this paper with the help of simulations.

ECCI has many advantages over transmission electron microscopy for the characterisation of crystal dislocations, e.g. easy sample preparation, larger examination area, etc~~.~~ [18]. However, it attracts less attention than TEM due to the relatively poor contrast. In early studies, a high-tilt imaging configuration ($50° - 70°$ tilt of the specimen stage) with the assistance of a backscattered electron detector ~~standing~~sited by the side of the specimen [6] was used to increase the total number of Back Scattered Electrons (BSEs~~.~~). This was considered a favourable arrangement because a large range of crystallographic directions can be reached simply by sample rotation, without changing the angle between the specimen surface and detector. This set-up, however, requires a special modification of the microscope. Instead of using the regular annular BSE detector, a rectangular BSE detector needs to be positioned by the side of the tilted specimen. Following technological developments concerning field emission guns with high probe current and of semiconductor backscattered electron detectors with high sensitivity, more convenient stage configurations are allowed. Significant work has been done by Crimp [10] [19] to simplify the imaging configurations.

In the study of dislocations in a shock loaded material, the dislocation density is very

sensitive to the parameters of the shock waves (loading duration, distance of wave propagation, release waves, etc.). The dislocation density in the shock loaded specimen is thought to depend on location. The measurement of dislocation density using TEM is not ~~possible~~feasible over such a large area and therefore ECCI is particularly beneficial for this type of study.

~~In~~In the work described in this paper, the backscattered electron detector is fixed under the pole piece, which is a popular and standard SEM configuration for metallurgical use. Shock induced dislocations in tantalum single crystals have here been studied using electron channelling contrast (ECC). The dislocations in the same area of a TEM foil are imaged using both TEM and electron channelling contrast imaging (ECCI) to investigate the visibility of the dislocations. The influence of imaging conditions (diffraction deviation parameter, depth of dislocation) on the contrast of the dislocations is studied. The contrast profiles of the dislocations are simulated using Matlab 2012b, using the formulae of Spencer et al. [5] and the results are compared with the experimental results. A methodology for dislocation density measurement in tantalum using ECCI is developed. The influence of SEM conditions on the imaging depth of the dislocations is discussed. An optimum choice of g vector and accelerating voltage is suggested.

Experimental method

Numerical simulation of dislocation contrast profiles in ECCI

The dislocation contrast profile (the backscattered electron intensity leaving the surface from a crystal containing a dislocation) is calculated following Spencer et al. [5], using two-beam theory and assuming the column approximation and isotropic elasticity. The equations used in the calculation are shown below, where equation (4) is taken from Spencer [5] and the remaining equations are from standard dynamical theory [~~17~~21].

$$\frac{d\psi_0}{dz} = -\frac{\pi}{\xi_0'}\psi_0 + \pi\left(\frac{i}{\xi_g} - \frac{1}{\xi_g'}\right)\psi_g \quad (1)$$

$$\frac{d\psi_g}{dz} = \pi\left(\frac{i}{\xi_g} - \frac{1}{\xi_g'}\right)\psi_0 + \left(-\frac{\pi}{\xi_0'} + 2\pi i\left(s + \frac{\alpha}{2\pi dz}\right)\right)\psi_g \quad (2)$$

$$\begin{pmatrix}\psi^{(1)}\\ \psi^{(2)}\end{pmatrix} = E^{-1}C^{-1}\begin{pmatrix}\psi_0(z)\\ \psi_g(z)\end{pmatrix} \quad (3)$$

$$I_B(0) = \sum_j I_B^{(j)}(0) = \frac{1}{1+p't}\left[p't + \sum_j\left(p^{(j)} - p'\right)\int_0^z I^{(j)}(z)dz\right] \quad (4)$$

$$E = \begin{pmatrix} exp\left(z\pi i\left(s - \sqrt{s^2 + 1/\xi_g^2}\right)\right) & 0 \\ 0 & exp\left(z\pi i\left(s + \sqrt{s^2 + 1/\xi_g^2}\right)\right)\end{pmatrix}$$

$$C = \begin{pmatrix} C_0^{(1)} & C_0^{(2)} \\ C_g^{(1)} & C_g^{(2)}\end{pmatrix} \quad (5)$$

ψ_0 and ψ_g in equations (1) and (2) are the transmitted and diffracted wave functions in the material. They are related to the absorption coefficients (ξ_0', ξ_g'), extinction distance (ξ_g), the phase angle of the strain field caused by the dislocation (α) and the depth of the wave inside the material (z). E and C represent matrices of the exponential terms and the diffraction coefficients C's, respectively. E and C are defined in Equation (5). Equation (3) is used to transform ψ_0 and ψ_g to the Bloch wave amplitudes, $\psi^{(1)}$ and $\psi^{(2)}$. The backscattered electron intensity leaving the entrance surface ($I_B(0)$) is a

function of the Bloch waves as shown in Equation (4).

The intensities of the backscattered electrons exiting the sample surface from all the columns were calculated and plotted as a dislocation profile. The reflection vector g used in the two beam experimental simulation is $\bar{2}11$, because it is a relatively low index g vector and easy to achieve under the current experimental conditions. The various parameters used in the simulation are shown in Table 1. In the examination of the effect of the deviation parameter, the depth of the dislocation beneath the crystal surface was fixed to be $0.2\xi_g$. To examine the effect of dislocation depth, the deviation parameter was set to 0. The absorption coefficients $\xi_0^{'}$ and $\xi_g^{'}$ are based on the work of Humphreys and Hirsch [~~19~~22].

Table 1. The parameters for the ECCI simulations

Dislocation depth $0.2\xi_g$	a	b	c
Deviation parameter w	0	±0.5	±1

Deviation parameter $w = 0$	a	b	c	d	e
Dislocation depth	0	$1\xi_g$	$2\xi_g$	$5\xi_g$	$10\xi_g$

Sample preparation

A single crystal tantalum disc with (111) entrance face was subjected to plate impact at a peak pressure of $6\ GPa$. The sample had diameter $12\ mm$ and thickness $4\ mm$. It was shock loaded using a $3\ mm$ thick tantalum projectile. A $1\ mm$ slice was taken from the front surface of the specimen using a spark erosion machine. A $3\ mm$ TEM disc was punched from the central area of the slice. This disc was then electro-polished in a solution of 5% HF, 95% methanol (volume percentage) at -10 ℃ and $25\ V$ voltage [~~16~~23].

Transmission electron microscopy

A JEOL 2100 TEM operating at $200\ kV$ was employed to characterise the shock induced dislocations in the $3\ mm$ tantalum disc. In the ~~thin~~electron transparent area, the dislocations were imaged using two-beam conditions. The Burgers vectors of the dislocations were determined using the $g \cdot b = 0$ extinction criterion and the direction of the dislocation line was determined using tilting experiments in the TEM.

Electron channelling contrast image

An electron channelling contrast image was acquired from both the 3mm TEM foil and the polished sample lateral surface using a Tescan Mira 3 SEM with a field emission gun and a retractable annular scintillator BSE detector under the pole piece. The imaging assembly is shown schematically in Figure 1. To maximise the signal received by the backscattered electron detector, the sample was brought to a position very close to the pole piece (5mm working distance). This means that the distance from the sample surface to the detector is about $3\ mm$ and that $\pm 5^{\circ}$ tilting is allowed. The sample was tilted slightly to set the crystal to the two-beam condition with $g = \bar{2}11$. The area on the $3\ mm$ disc imaged by TEM was imaged in the SEM using backscattered electrons. The images were stitched together and compared with the TEM image.

Results

Simulation of the electron channelling contrast profile across a dislocation (planar incident wave)

Figure 2(a) shows the intensity profile calculated across the $g = \bar{2}11$ channelling pattern lines in tantalum. The main features: bright region with $w < 0$ and a dark line positive of Bragg condition, are in agreement with Spencer et al. [5] (calculation using ~~many~~mutiple beam theory) and experimental channelling patterns [3~~,~~] [4~~,~~] [5]. Figure 2(b) shows the backscattering coefficients $p^{(j)}$ around the Bragg

condition. Bloch wave 1 is backscattered more at the Bragg condition while Bloch wave 2 is backscattered less. This also agrees with Spencer et al [5].

A simulated profile of backscattered electron intensity across a screw dislocation in a semi-infinite tantalum crystal at a depth of $0.2\xi_g$ beneath the crystal surface is shown in Figure 3. The crystal was set to the Bragg condition for $\bar{2}11$. The extinction distance ξ_g for this condition is calculated to be 18 nm at 30 kV beam voltage [~~17] [18~~21] [24]. The strain field of the dislocation has altered the intensity of the backscattered electrons. The BSE intensity on the right side of the dislocation is lower than the average background intensity. On the left side, the intensity is higher than the background. The peak and valley (the positive and negative part of the dislocation profile) have widths of about one ξ_g each, which means that the total width of the dislocation profile simulated here is about $2\xi_g$.

The effect of the deviation parameter w ($w = s\xi_g$) was investigated by plotting the BSE profiles across the dislocation for different deviation parameters. Figure 4 shows plots across a screw dislocation in Ta, at depth $0.2\xi_{211}$ and with w equal to -1, -0.5, 0, 0.5 and 1. The intensity of the profile with $w = 0$ is symmetrical about the background intensity. It is obvious that the dislocation contrast is highest at the exact Bragg condition. The channelling pattern 'rocking curves', the backscattered electron profile across a dislocation and the effect of deviation parameter on the dislocation contrast are consistent with the results of Spencer et al. [5] and Wilkinson et al. [8].

In an examination of the effect of dislocation depth, the deviation parameter w was set to 0. The profiles are shown in Figure 5. All the plots have the same background intensity. The width of the dislocation image becomes slightly smaller as the dislocation position become deeper in the material, but is still within a range of around $2\xi_g$. The contrast of the dislocation gradually attenuates with increasing depth. ~~The thickness range of~~Because, however, the ~~visibility is worked out from the experiment and will will be discussed in the discussion section. This is because the criterion for~~dislocation visibility depends on many instrumental parameters~~ and~~, it is not possible to predict, *a*

Formatted: Font: Italic

priori, the cut-off depth. This is more easily determined experimentally and will be discussed later.

Comparison of dislocation images in TEM and ECCI

A TEM micrograph of the shock-loaded tantalum is shown in Figure 6a. Most of the dislocations in the specimen form a tangled structure with some loops/debris and individual dislocation lines in between. The same thin area of this TEM foil was examined by ECCI. Because the signal of the backscattered electrons ~~(which is the signal used in ECCI)~~ is influenced by the specimen thickness, the brightness of the background of the electron channelling contrast image varies strongly across the image This makes it difficult to optimise the contrast of all the dislocations in the image at the same time. Therefore, multiple images were taken across the same area and stitched together. The stitched electron channelling contrast image is shown in Figure 6b. The image has been ~~reversed~~inverted for easier comparison with the TEM micrograph. For better demonstration of the dislocation contrast in ECCI, an ECCI image taken from a bulk specimen is shown in Figure 6c, which shows better contrast for dislocations because the electrons are backscattered from a thick (bulk) specimen and the background intensity is constant. The dislocation contrast in ECCI is not as strong as in the TEM bright field image. There is a large number of dislocations in the TEM images absent in the ECC image. However, all the ECC imaged dislocations appear in the TEM image, i.e. the remaining dislocation images show good agreement with the TEM bright field image. For example, as shown in the higher magnification Figure 7a, part of dislocation A appears as line A′ in the ECCI in Figure 7b, where the contrast has been enhanced.

Burgers vector analysis in the TEM indicates that the dislocation A has Burgers vector $\frac{1}{2}[11\bar{1}]$. Tilting experiments in the TEM employed to determine the slip plane of the dislocations suggest that dislocation A has slip plane (101) and dislocation line direction $[11\bar{1}]$, which is parallel to the Burgers vector direction. Therefore, dislocation

A is mainly screw type, which is the same type as used for the calculations in the previous section.

Only part of the dislocation line appears in the ECC image, as shown in Figure 7b. The visible dislocation line has a length of $200\ nm$ only. However, the total length of the dislocation is greater than $400\ nm$. This is due to the effective penetration depth of the $30kV$ electrons in the SEM being smaller than the depth that can be seen in the TEM. The average imaging depth measured from ECCI is around $6\xi_g$ ($100-140\ nm$) for a 112 g vector.

The effect of the deviation parameter on the dislocation image

To help optimise the dislocation contrast in ECCI, the effect of the deviation parameter was investigated experimentally by taking an image of the same area using a range of beam directions with the same g vector. The contrast of the dislocations was then measured as the intensity of the peak divided by the background intensity of the ECCI.

The influence of the deviation parameter is shown in Figure 8, in which all the images were obtained experimentally at $30kV$. The y axis is the contrast of the dislocation images on the grey scale. The x axis is the deviation parameter w. When $w = 0$ the beam direction is exactly at the Bragg condition for the $\bar{2}11$ reflection. It can be seen that the contrast is low at negative s, increases with deviation parameter up to the Bragg condition and decreases subsequently with s when s is positive. The maximum dislocation contrast is at the exact Bragg condition. From the actual images it is found that when the beam direction is around 0.5^{c} ($w \approx 1$) within the exact Bragg condition of $\bar{2}11$ reflection, the contrast of the dislocation is acceptable.

The effect of voltage and reflection plane

The influence of voltage on the visibility of the ECCI images has been calculated. To make the results more realistic the beam has been made conically

convergent with a half angle of $0.25°$. The results for g vector $\bar{2}11$ are shown in Figure 9. Since the dislocation contrast falls off with depth, different dislocation depths are used in the simulation. The contrast of the dislocations generally increases with accelerating voltage.

The effect of using different g vectors on the dislocation contrast is shown in Figure 10. Low index g vectors give better contrast and penetration than the higher index reflections.

The effect of Z

The effect of the atomic number Z on the dislocation contrast in ECCI was studied by performing the simulation on aluminum using 30 kV and 111 g vector. The extinction distance at this condition is 32 nm, similar to the 123 g vector in tantalum. While the ECCI mechanism provides a slightly larger difference in intensity between the dislocation and the background in aluminum, the absolute magnitude is far smaller due to a smaller backscattering coefficient, requiring a far higher beam current to provide a sufficiently bright image. If intensity is limiting, the penetration depth is $8\xi_g$ or 250 nm. If contrast is limiting, the penetration depth is far more than this. This is an experimental question and the answer will depend rather on the exact microscope and detector being used.

Dislocation density measurement

The dislocation density in the imaged area was measured by counting the number of dislocation terminations on the TEM bright field image. In Figure 7 it is $3.6\times10^{13}m^{-2}$. The dislocation density measured by ECCI using the same method is $3.4\times10^{13}m^{-2}$. Several lines were drawn on the electron channelling contrast image. The dislocations crossed by these lines were counted (as N). The average dislocation density is then $n = \frac{N}{dL}$, where d is the imaging depth of the ECCI and L is the total length of these lines. The maximum imaging depth of ECCI for Ta $\bar{2}11$ is known to be $\sim 110\ nm$ in the current set-up. The densities of the dislocations were then calculated using this

depth. The density measured by this method was $4.0\times10^{13}m^{-2}$. In practice, the first method (i.e. counting dislocation ends) is recommended since the imaging depth of the dislocations could vary.

Discussion

The calculations suggest that dislocations in tantalum should indeed be visible using the backscattered electron signal. The background change with the deviation parameter w is essentially due to the change of the backscattering coefficient $p^{'}$. The background intensity is $I_B(0)$ without the term related to the sum of the Bloch waves, i.e. $p^{'}/(1+p^{'}t)$ [5]. The backscattering coefficient $p^{'}$ is a function of the Fourier coefficients $C_g^{(i)}$ and hence is related to the deviation parameter w. The width of the dislocation image is around 2 times the extinction distance, which is in good agreement with previous simulation results [5,8,9]. The 'oscillatory' shape of the profile comes from the $g\cdot b$ component. When the sample column is on either side of the dislocation the $g\cdot b$ component will have a different sign. This will give a positive/negative gain to the Bloch wave intensity and hence have a different influence on the backscattered electron intensity.

The dislocation depth has a strong effect on the image contrast. The contrast falls exponentially with dislocation depth. Superimposed on this exponential attenuation, the contrast will also oscillate with depth, with a periodicity of ξ_g [5]. The contrast of the dislocation (I_{max}-I_{min}) reduces as the depth of the dislocation in the material increases. In Equation (4), the contrast of the dislocation in the ECCI comes from the sum of the integration of the Bloch waves intensities with depth. The Bloch waves attenuate quickly with crystal depth due to absorption. When the dislocation is close to the surface, the Bloch waves are still strong when they are altered by the strain field of the dislocation core, hence altering significantly the backscattered electron intensity. When the dislocation is deep inside the crystal, the Bloch waves are influenced by the dislocation core when they are weak and thus barely change the total $\int I_j\,dz$ term.

Therefore the dislocation contrast is much smaller than when the dislocation is close to the surface.

The ECCIs of the dislocations were taken in an SEM with a normal configuration (low angle tilt). The same area was examined by TEM and compared with ECCI. At first glance, the dislocation micrographs from ECCI look completely different from the TEM bright field images. The dislocation images in ECCI are not as dense or clear. However, those dislocations which do appear in ECCI show good agreement with the bright-field images. Some dislocations may be missing because their depth is greater than the imaging depth of the backscattered electrons (here around 100 nm). If 100 nm is used as a criterion for invisibility of dislocations with g vector $\bar{2}11$, the imaging depth of dislocations in other conditions can be estimated by comparing the dislocation contrast from the simulation. In this case, the calculated dislocation contrast for g=$\bar{2}11$ with the dislocation at 100 nm deep is 0.0003 (as shown in Figure 10) and the conditions under the dashed line can be treated as invisible because they have too low contrast. This means, for example, that the 123 reflection would not show any contrast for dislocations under 30kV for any practicable dislocation depth. The low index g vectors have higher imaging depth than the high index reflections. The contrast of dislocation images with the 110 reflection, although decreasing with dislocation depth, is still higher than 0.0003 (criterion of visibility) when the dislocation is 100 nm deep in the crystal. The maximum imaging depth for the g vector 110 is around $15\xi_g$ (i.e. $150\ nm$) compared with $6\xi_g$ ($100\ nm$) for reflection $\bar{2}11$. This is due to the fact that electrons are less anomalously absorbed when travelling through the crystal when g is large (ξ_g/ξ_g' increases with g vector) [~~19~~22] and therefore not enough electrons are backscattered to provide sufficient contrast. Also, the convergence angle in the SEM corresponds to a smaller deviation parameter when g is low index. This means, when integrating over the electron intensity, that a higher proportion of the integral comes from near Bragg, where the contrast is strongest. Conversely, high index g vectors have a greater deviation parameter range, meaning that a greater proportion of the integral comes from regions

where the dislocation contrast is weak. Thus the reason why low index g vectors give high contrast is simply that the lower index crystal planes are stronger reflections. Figure 9 shows that the imaging depth for lower voltage electrons is smaller than for 30kV. For example, at 20kV, dislocations at 100 nm will be invisible for $\bar{2}11$ g vector, at 10kV dislocations at 80 nm will not show contrast in ECCI.

A previous study by Ahmed and Simkin suggested that the dislocation contrast is optimised at the Bragg condition [12,13]. We would not disagree with this. The influence of the deviation parameter w on the contrast profile is shown in Figure 8 and Figure 4(b). The total range of acceptable contrast is around $\pm 0.5°$. In the simulation, the contrast decreases more rapidly when w is higher than 0 ~~compare~~compared with the experimental results in Figure 8. But even when the electron beam is tilted $0.25°$ away from the Bragg condition, part of the beam in the range will still stay close to the Bragg condition and give rise to dislocation contrast. This is why the contrast for the dislocations in ECCI appears larger than the theoretical value when w is higher than zero, and drops quickly when the beam direction is out of the range of beam convergence half angle ($0.25°$) from the exact Bragg condition. Although it seems that large electron convergence angle can provide a large range of dislocation imaging directions, in practice it is still recommended that a small convergence angle should be used. This is because a small convergence angle allows a higher fraction of the beam to stay close to the Bragg condition and ~~provide~~provides the strongest contrast.

The dislocation density measured by ECCI is accurate when compared with the TEM measurement. In the preparation of the TEM foil, dislocations can escape out of the specimen from the thin area. These escapes would certainly reduce the dislocation density measured by TEM, but are less likely in the ECCI measurement, because the strain is more difficult to release from a bulk sample than from a thin foil.

This technique has been exploited to examine the large scale variation of defect densities in shocked tantalum single crystals (Pang et al.) (to be published). An example

is shown in Figure 11.

~~Conclusion~~

Conclusions

The contrast profile for a dislocation in an electron channelling contrast image has been calculated. The results indicate that in an SEM with an untilted sample, dislocations in a tantalum specimen should be visible in the backscattered electron image near the Bragg condition. A conventional BSE detector assembly is adequate for imaging dislocations. The method for measuring the dislocation density using ECCI can thus be summarised to be: use a small working distance to maximise the collection angle of the backscattered electrons~~,~~; use a small convergence of the electron beam~~,~~; use the exact Bragg condition to optimise the dislocation contrast; use as high an accelerating voltage as possible; use the lowest index reflection plane. This will provide the highest dislocation contrast and greatest imaging depth.

Acknowledgement

We would like to thank Colin Humphreys and Mark Twigg for help concerning the diffraction calculations, Mike Mills for his interest and for a very useful conversation in Oxford and Gareth Douglas for help with the programming. We would also like to acknowledge some very helpful comments by an anonymous referee.

References

[1] D.E. Newbury, D.C. Joy, P. Echlin, C.E. Fiori and J.I. Goldstein, *Electron channeling contrast in the SEM*, in *Advanced Scanning Electron Microscopy and X-ray Microanalysis*, D.E. Newbury, D.C. Joy, P. Echlin, C.E. Fiori and J.I. Goldstein, eds., Springer US, New York, 1986, pp. 87-145.

[2] P.B. Hirsch, A. Howie and M.J. Whelan, *On the production of X-rays in thin metal foils*, Phil. Mag. 7 (1962), pp. 2095-2100.

[3] D.G. Coates, *Kikuchi-like reflection patterns obtained with the scanning electron microscope*, Phil. Mag. 16 (1967), pp. 1179-1184.

[4] P.B. Hirsch and C.J. Humphreys, *The dynamical theory of scanning electron microscope channelling patterns*, Proceedings of Third Annual Scanning Electron Microscope Symposium, Chicago, 1970.

[5] J.P. Spencer, C.J. Humphreys and P.B. Hirsch, *A dynamical theory for the contrast of perfect and imperfect crystals in the scanning electron microscope using backscattered electrons*, Phil. Mag. 26 (1972), pp. 193-213.

[6] P. Morin, M. Pitaval, D. Besnard and G. Fontaine, *Electron–channelling imaging in scanning electron microscopy*, Phil. Mag. A. 40 (1979), pp. 511-524.

[7] J.T. Czernuszka, N.J. Long, E.D. Boyes and P.B. Hirsch, *Imaging of dislocations using backscattered electrons in a scanning electron microscope*, Phil. Mag. Lett. 62 (1990), pp. 227-232.

[8] A.J. Wilkinson, G.R. Anstis, J.T. Czernuszka, N.J. Long and P.B. Hirsch, *Electron channelling contrast imaging of interfacial defects in strained silicon-germanium layers on silicon*, Phil. Mag. A. 68 (1993), pp. 59-80.

[9] A.J. Wilkinson and P.B. Hirsch, *The effects of surface stress relaxation on electron channelling contrast images of dislocations*, Phil. Mag. A 72 (1995), pp. 81-103.

~~[10~~[10] M.A. Crimp, B.A. Simkin and B.C. Ng, *Demonstration of the $g \cdot b \times u = 0$ edge dislocation invisibility criterion for electron channelling contrast imaging*, Phil. Mag. Lett. 81 (2001), pp. 833-837.

[11] Y.N. Picard, M.E. Twigg, J.D. Caldwell, C.R. Eddy, M.A. Mastro and R.T. Holm, *Resolving the Burgers vector for individual GaN dislocations by electron channeling contrast imaging*, Scr. Mater. 61 (2009), pp. 773-776.

~~[11] M.A. Crimp, B.A. Simkin and B.C. Ng, *Demonstration of the g · b × u = 0 edge dislocation invisibility criterion for electron channelling contrast imaging*, Phil. Mag. Lett. 81 (2001), pp. 833-837.~~

[12] B.A. Simkin and M.A. Crimp, *An experimentally convenient configuration for electron channeling contrast imaging*, Ultramicroscopy. 77 (1999), pp. 65-75.

[13] J. Ahmed, A.J. Wilkinson and S.G. Roberts, *Characterizing dislocation structures in bulk fatigued copper single crystals using electron channelling contrast imaging (ECCI)*, Phil. Mag. Lett. 76 (1997), pp. 237-246.

~~[14~~[14] R. Zauter, F. Petry, H.J. Christ and H. Mughrabi, *High temperature creep behaviour and microstructure development of AISI 304L stainless steel*, Mater. Sci. Eng., A 124 (1990), pp. 125-132.

[15] R. Zauter , F. Petry , M. Bayerlein , C. Sommer , H.J. Christ and H. Mughrabi, *Electron channelling contrast as a supplementary method for microstructural investigations in deformed metals*, Phil. Mag. 66 (1992), pp. 425-436.

[16] A. Weidner, F. Pyczak and H. Biermann, *Scanning and transmission electron microscopy investigations of defect arrangements in a two-phase β-TiAl alloy*, Mater. Sci. Eng., A 571 (2013), pp. 49-56.

[17] A. Weidner and H. Biermann, *Case studies on the application of high-resolution electron channelling contrast imaging – investigation of defects and defect arrangements in metallic materials*, Phil. Mag. 95 (2015), pp. 759-793.

[18] S. Zaefferer and N. Elhami, Theory and application of electron channelling contrast imaging under controlled diffraction conditions, Acta. Mater. 75 (2014), pp. 20-50.

[19] M.A. Crimp, *Scanning electron microscopy imaging of dislocations in bulk materials, using electron channeling contrast*, Microsc. Res. Techniq. 69 (2006), pp. 374-381.

[~~15~~20] I. Gutierrez-Urrutia and D. Raabe, *Dislocation density measurement by electron channeling contrast imaging in a scanning electron microscope*, Scr. Mater. 66 (2012), pp. 343-346.

~~[16~~[21]P.B. Hirsch, A. Howie, R.B. Nicholson, D.W. Pashley, M.J. Whelan and L. Marton, *Electron Microscopy of Thin Crystals*, Butterworths, London, 1977.

[22] C.J. Humphreys, P.B. Hirsch, *Absorption parameters in electron diffraction theory*, Phil. Mag. 18 (1968), pp. 115-122.

[23] L.E. Murr, M.A. Meyers, C.S. Niou, Y.J. Chen, S. Pappu and C. Kennedy, *Shock-induced deformation twinning in tantalum*, Acta. Mater. 45 (1997), pp. 157-175.

~~[17] P.B. Hirsch, A. Howie, R.B. Nicholson, D.W. Pashley, M.J. Whelan and L. Marton, *Electron Microscopy of Thin Crystals*, Butterworths, London, 1977.~~

~~[18~~ [24] E. Prince, *International Table for Crystallography, Mathematical, Physical and Chemical Tables*, Springer Science & Business Media, 2004.

~~[19] C.J. Humphreys, P.B. Hirsch, *Absorption parameters in electron diffraction theory*, Phil. Mag. 18 (1968), pp. 115-122.~~

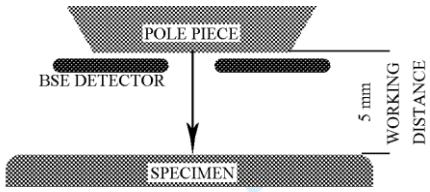

Figure 1 The imaging configuration for the tantalum single crystals

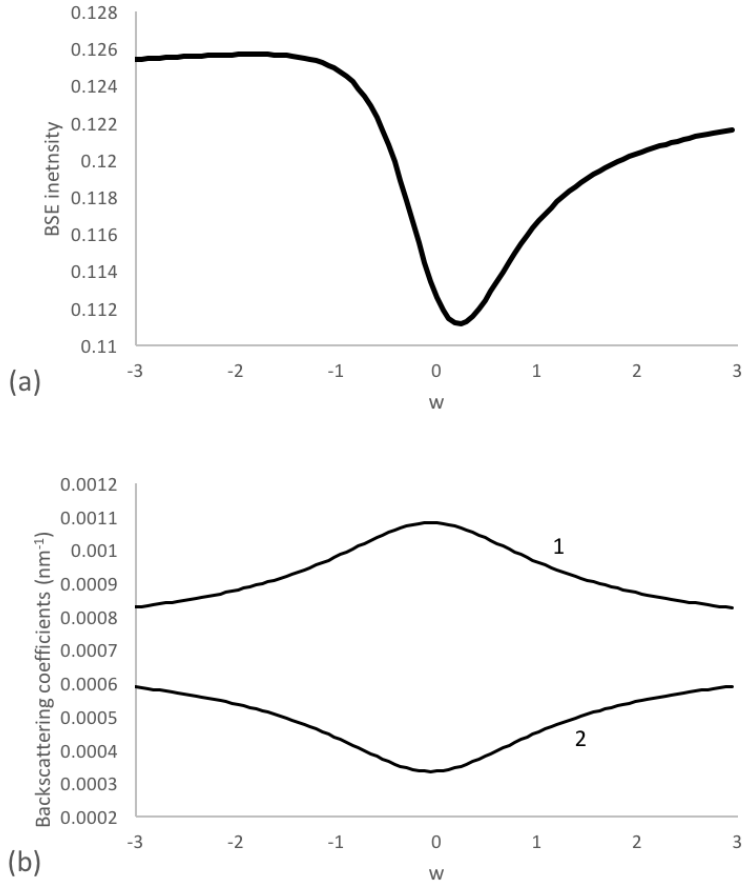

Figure 2 (a) The backscattered electron intensity around the Bragg condition for g vector $\bar{2}11$; (b) The backscattering coefficients for Bloch waves 1 and 2 with respect to w.

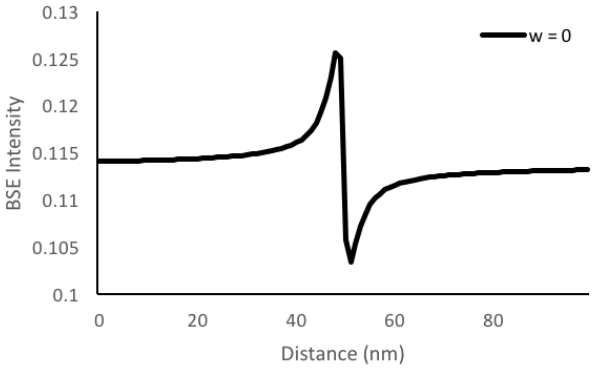

Figure 3 The profile across a screw dislocation simulated with w=0, dislocation depth $0.2\xi_g$. $g \cdot b = 1$.

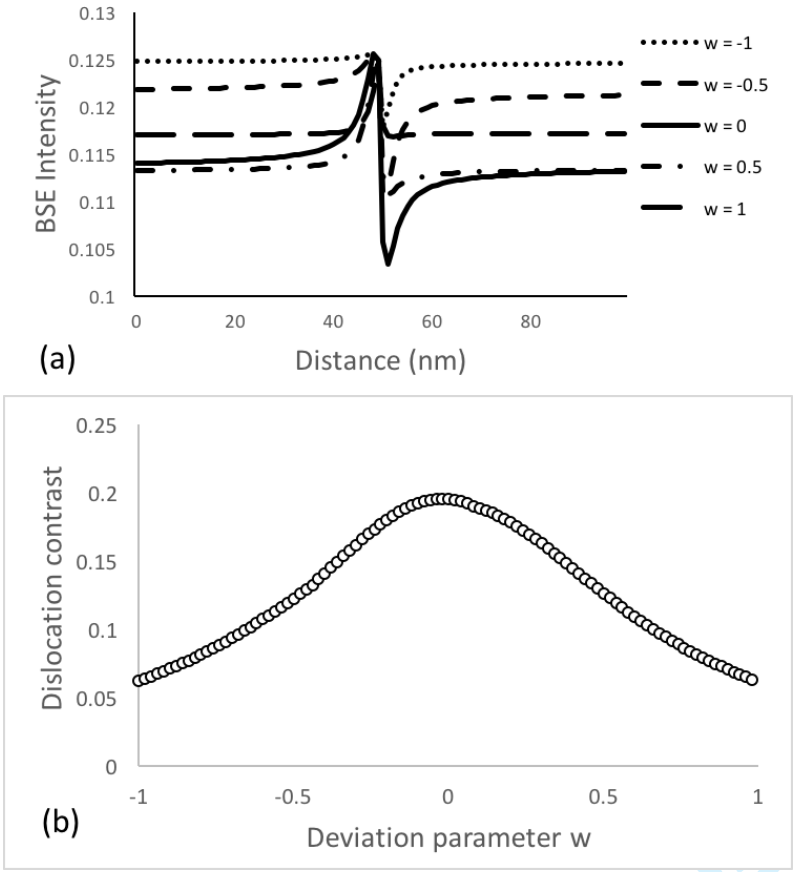

Figure 4 (a) BSE intensity profiles across a screw dislocation for various deviation parameters w, dislocation depth $0.2\xi_g$, $g \cdot b = 1$; (b) Effect of deviation parameter on the dislocation contrast (simulation results)

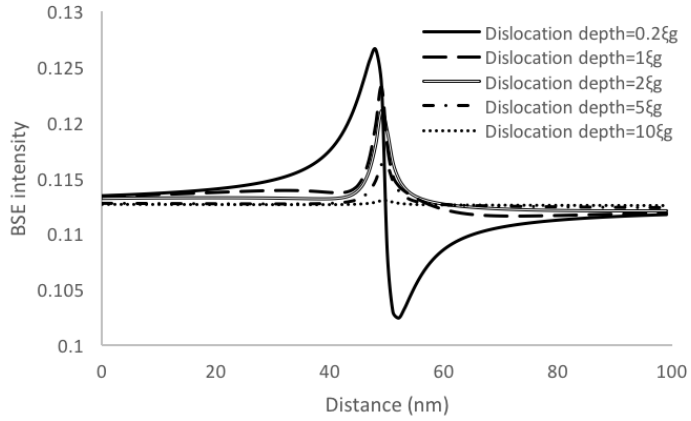

Figure 5 BSE intensity profile across a screw dislocation at various depths, $g \cdot b = 1$.

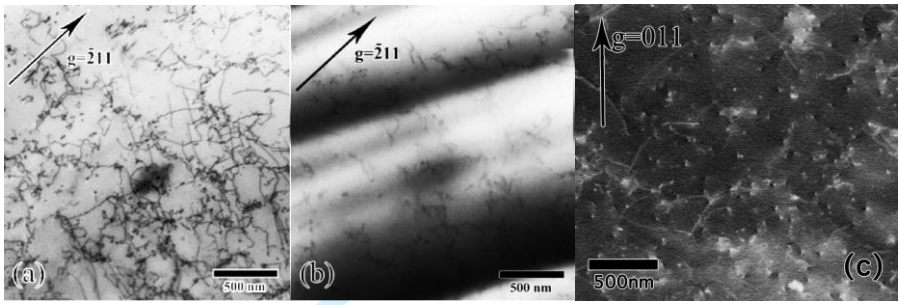

Figure 6 (a) TEM micrograph of the dislocations in a shock loaded tantalum single crystal with loading direction [111]; (b) ECCI of dislocations in the same area as (a). The discontinuities across the image are a result of the image stitching; (c) an ECCI image of dislocations in a shock loaded bulk tantalum specimen.

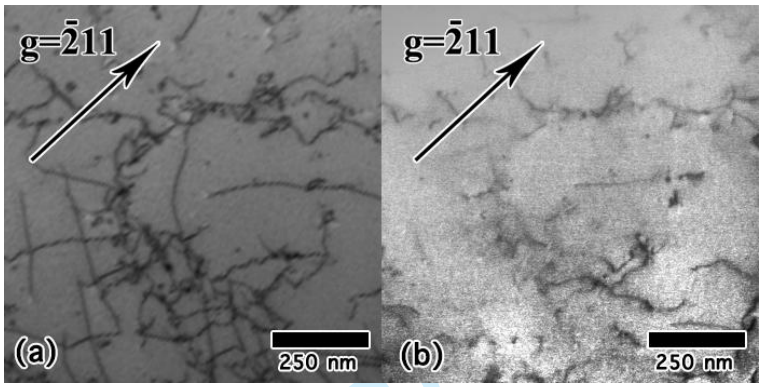

Figure 7 (a) Dislocation micrographs showing detailed one-to-one correspondence between dislocation image in TEM and ECCI (a) TEM (b) ~~processed~~inverted ECCI.

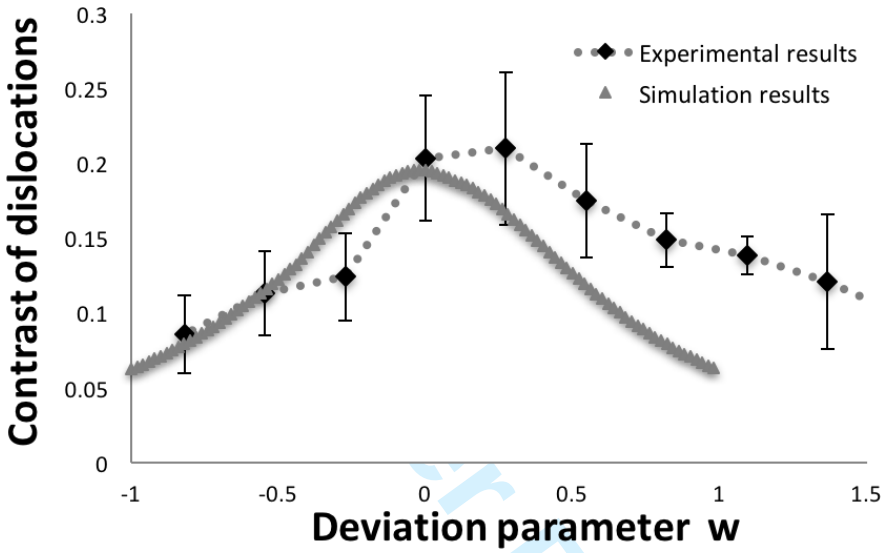

Figure 8 The influence of deviation parameter on the contrast of dislocations in ECCI (experimental data). The square ~~sign shows~~symbols relate to the simulation results from Figure 4(b).

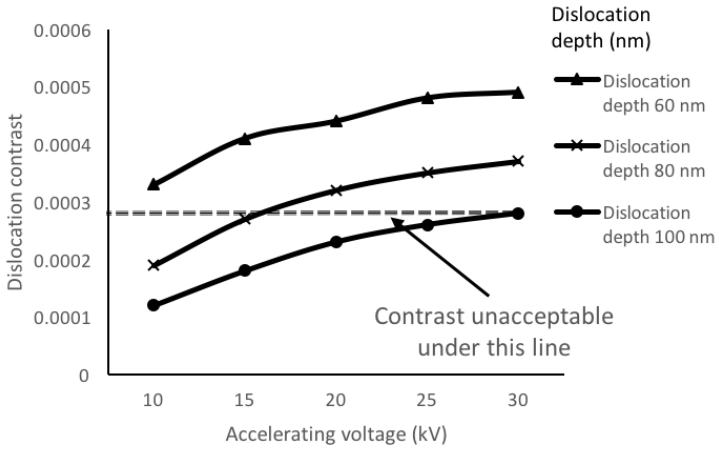

Figure 9 The influence of accelerating voltage on the contrast of dislocations with a variety of depths. The dislocation contrast is calculated by (Maximum brightness – Minimum brightness)/ Maximum brightness in a simulated profile. The conical beam convergence half angle used in the calculation is 0.25°.

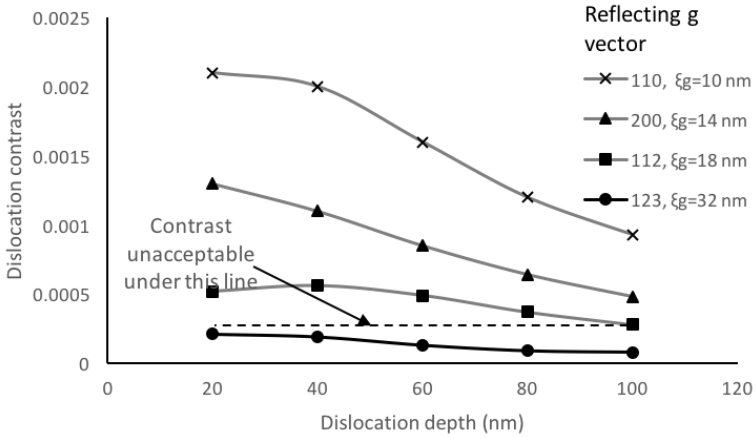

Figure 10 The effect of using different g vectors on the contrast of dislocations with a variety of depths. The dislocation contrast is calculated by (Maximum brightness – Minimum brightness)/ Maximum brightness in a simulated profile. The conical beam convergence half angle used in the calculation is 0.25°.

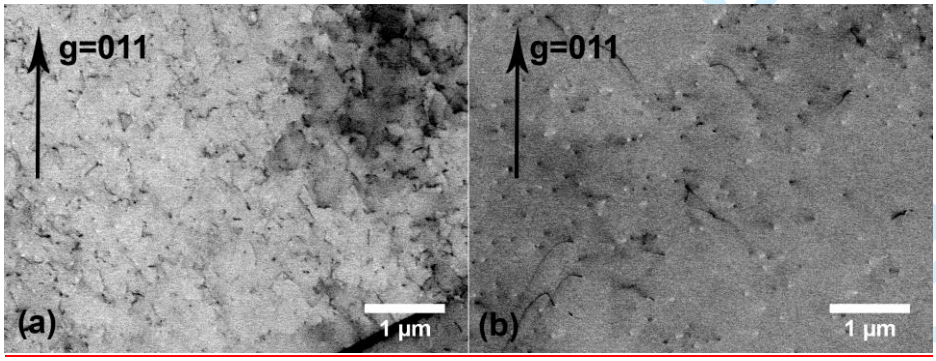

Figure 11 ECCI of two regions of a shocked tantalum specimen (a) front (b) rear. ECCI enabled the dislocation content (density and nature) to be determined over large area of macroscopic specimen (Pang et.al. (to be published)).